

# BPSK and PAM Modulation in a Single-drive Push-pull Silicon Michelson Interferometric Modulator

Minjuan Wang, Linjie Zhou\*, Yanyang Zhou, and Jianping Chen

State key Laboratory of Advanced Optical Communication Systems and Networks,  
Department of Electronic Engineering, Shanghai Jiao Tong University, Shanghai 200240, P. R. China  
\*ljzhou@sjtu.edu.cn

**Abstract:** 20 Gbaud/s PAM-4 and 28 Gb/s BPSK modulation are demonstrated in a single-drive push-pull silicon Michelson interferometric modulator with  $\sim 3$  dB on-chip insertion loss. The modulator features a compact size and a high extinction ratio.

**OCIS codes:** (130.4110) Modulators; (230.2090) Electro-optical devices; (130.3120) Integrated optics devices

## 1. Introduction

Silicon-based modulators have developed rapidly in the last couple of years, with ultra-high data rates up to 60 Gb/s for on-off keying (OOK) modulation in a resonator structure [1] and 70 Gb/s in a Mach-Zehnder interferometer (MZI) structure [2-3]. Advanced modulation formats together with polarization division multiplexing have been achieved in a silicon optical modulator with a data rate of 112 Gb/s for coherent optical communications [4]. The high-order modulation formats can provide a higher spectral efficiency, lowering the bandwidth requirement at the same data rate. The 4-level pulse amplitude modulation (PAM-4) has become a promising alternative to substitute the OOK modulation for the next generation optical networks [5]. Recently, Michelson interferometric (MI) modulator is put forward as one of the candidates for its high modulation efficiency and compactness [6-7].

In this paper, we demonstrate a silicon MI modulator with its reflection enabled by Sagnac loop reflectors connected to the end of each arm. The propagating light makes a round trip along the phase-shifting waveguides, and thus the RF signal interacts with both forward and backward light wave, leading to enhanced modulation efficiency. As the phase shifter length is reduced by half, the modulator becomes more compact, in favor of integration in a large-scale photonic integrated circuit (LS-PIC). Moreover, as light is split and combined using the same 3-dB coupler, the static extinction ratio (ER) is high due to the complete destructive interference, unaffected by the splitting ratio of the coupler. Preliminary measurements show that the MI modulator can achieve 20 Gbaud/s PAM-4 and 28 Gb/s BPSK modulation.

## 2. Device structure

Figure 1(a) shows the schematic of the single-drive push-pull MI modulator, which consists of one 3-dB  $2 \times 2$  multimode interferometer (MMI) coupler and two imbalanced arms terminated with two identical Sagnac loop reflectors, separately. The arm length difference is  $180 \mu\text{m}$ . Each arm contains a 1-mm-long phase shifter based on a p-n junction working in the carrier depletion mode. Figure 1(b) shows the cross-section of the active arms along the dashed line in Fig. 1(a). Ridge-type SOI waveguides are used with the width  $500 \text{ nm}$ , height  $220 \text{ nm}$ , and slab thickness  $60 \text{ nm}$ . The p-type and n-type doping concentrations in the p-n junctions are  $\sim 2 \times 10^{17} \text{ cm}^{-3}$  and  $\sim 4 \times 10^{17} \text{ cm}^{-3}$ , respectively. The heavily  $p^+$  doping regions are positioned in the slab outside the MI arms and connected to the signal (S) and ground (G) metal lines of the traveling-wave electrode (TWE). While the heavily  $n^+$  doping region is in the middle of the two arms and connected to the DC bias metal pad.

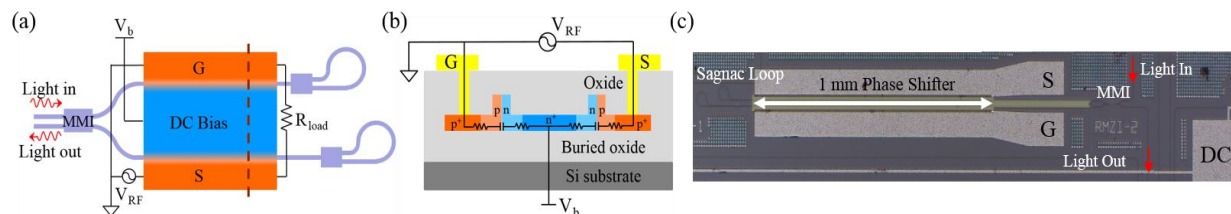


Fig. 1 (a) Schematic of the MI modulator. (b) Cross-sectional view of the Michelson interferometer modulation arms. (c) Optical microscope image of the fabricated device.

## 3. Experimental Results

Figure 2(a) shows the normalized transmission spectra under various reverse bias voltages applied on the shorter arm of the MI modulator. The fiber-to-fiber insertion loss is  $\sim 8$  dB, consisting of  $\sim 3$  dB on-chip insertion loss and

~2.5 dB coupling loss per facet. The free spectral range (FSR) is 3.22 nm and the static ER before tuning is more than 30 dB, as shown in the inset of Fig. 2(a). The high ER is one of the merits intrinsic to MI, and therefore MI has a much higher tolerance to the uneven splitting ratio of the coupler compared to a Mach-Zehnder interferometer. Figure 2(b) shows the phase shift changing with the bias voltage deduced from Fig. 2(a). The  $V_{\pi}L$  was calculated to be 0.95-1.26 V cm in the range of 1 V to 8 V. Figure 2(c) shows the electro-electro (EE)  $S_{21}$  responses of the TWE measured by a vector network analyzer (VNA) at various DC biases. The EE  $S_{21}$  6-dB bandwidth increases with reverse bias and exceeds the maximum measured range of 40 GHz. It should be noted that the microwave and the optical wave travel in the opposite directions after optical reflection, lowering the modulation efficiency at the high frequency end.

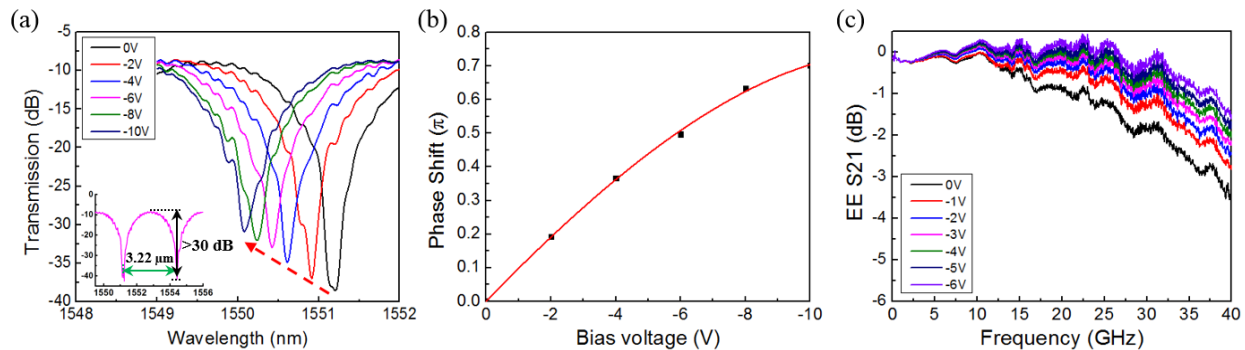


Fig. 2 (a) Transmission spectra under various reverse bias voltages. The inset shows the passive spectrum covering one FSR. (b) Phase shift as a function of reverse bias voltage. The red line is a fitting curve. (c) Measured EE  $S_{21}$  responses of the TWE.

The BSPK and PAM modulation experiments were carried out using our modulator. A 28 Gb/s pseudo-random binary sequence (PRBS) signal with a length of  $2^{31}-1$  generated by a pulse pattern generator (PPG) was first amplified to a peak-to-peak voltage ( $V_{pp}$ ) of 7 V before applied onto the TWE via a 40 GHz GS microprobe. The TWE was terminated with an external 50 ohm resistor. Figs. 3(a)-3(d) show the measurement results. A clear constellation diagram was observed with an error vector magnitude (EVM) of 22.3%. A 20 GHz arbitrary waveform generator (AWG) was used to generate the PAM-4 RF drive signal. Figs. 3(e) and 3(f) show the measured 18 and 20 Gbaud/s PAM-4 eye diagrams, respectively. Four signal levels can be clearly discerned from the eye diagrams.

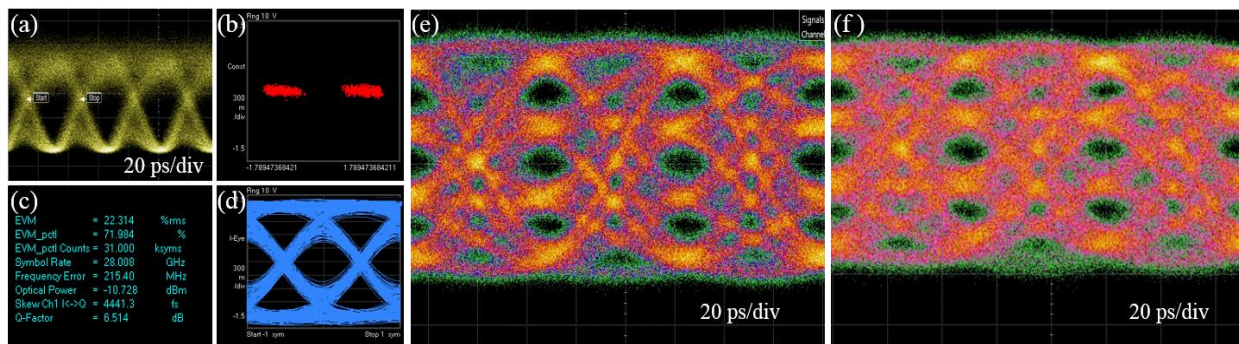


Fig. 3 (a)-(d) Measurement results for the 28 Gb/s BPSK modulation with (a) eye diagram, (b) constellation diagram, (c) performance summary, and (d) demodulated eye diagram. (e) and (f) Eye diagrams for the PAM-4 modulation with symbol rates of (e) 18 Gbaud/s and (f) 20 Gbaud/s.

#### 4. References

- [1] X. Xiao, et al., "60 Gbit/s silicon modulators with enhanced electro-optical efficiency," in Optical Fiber Communication Conference 2013, Anaheim, California United States, pp. OW4J. 3 (2013).
- [2] H. Xu, et al., "High-speed silicon modulator with band equalization," *Opt. Lett.* **39**, 4839-4842 (2014).
- [3] W. Heni, et al., "Plasmonic Mach-Zehnder Modulator with > 70 GHz Electrical Bandwidth Demonstrating 90 Gbit/s 4-ASK," in Optical Fiber Communication Conference 2015, Los Angeles, California United States, pp. Tu2A. 2 (2015).
- [4] P. Dong, et al., "112-Gb/s monolithic PDM-QPSK modulator in silicon," *Opt. Express* **20**, B624-B629 (2012).
- [5] IEEE P802.3bs 400GbE Task Force, <http://www.ieee802.org/3/bs/public>.
- [6] X. Li, et al., "Highly efficient silicon Michelson interferometer modulators," *IEEE Photon. Technol. Lett.* **25**, 407-409 (2013).
- [7] D. Patel, et al., "High-speed compact silicon photonic Michelson interferometric modulator," *Opt. Express* **22**, 26788-26802 (2014).